Prognostic index of immune-related lncRNAs for immunotherapy responsiveness and chemotherapy sensitivity in ovarian cancer patients

Xinxin Xu[1,2], Chen Zhang[2]*, Lingfei Han[1,3]*

[1]Department of Gynecology, Shanghai Tenth People's Hospital, Tongji University School of Medicine, Shanghai, China
[2]School of Medicine, Tongji University, Shanghai, China
[3]Department of Gynecology, Shanghai Key Laboratory of Maternal Fetal Medicine, Shanghai Institute of Maternal-Fetal Medicine and Gynecologic Oncology, Shanghai First Maternity and Infant Hospital, School of Medicine, School of Life Science and Technology, Tongji University, Shanghai, China

Submitted: 22 August 2025; **Accepted:** 19 November 2025
Online publication: 15 January 2026

Arch Med Sci
DOI: https://doi.org/10.5114/aoms/214432

***Corresponding authors:**
Lingfei Han
Department of Gynecology
Shanghai Tenth
People's Hospital
Tongji University
School of Medicine
No. 301, Yanchang
Middle Road
Shanghai 200000, China
Department of Gynecology
Shanghai Key
Laboratory of Maternal
Fetal Medicine
Shanghai Institute
of Maternal-Fetal
Medicine and
Gynecologic Oncology
Shanghai First
Maternity and
Infant Hospital
School of Medicine
School of Life Science
and Technology
Tongji University
No. 2699, Gaoke
West Road
Pudong New Area
Shanghai 200092, China
E-mail: lingfeihan@tongji.edu.cn

Chen Zhang
School of Medicine
Tongji University
No. 1239, Siping Road
Yangpu District
Shanghai 200092, China
E-mail: chenzhang@tongji.edu.cn

Abstract

Introduction: Ovarian cancer (OV), ranking among the most lethal gynecologic malignancies, is characterized by elevated mortality rates primarily attributable to immature diagnostic tools and the insensitivity of chemotherapy. Despite the impressive success of immune checkpoint inhibitor (ICI) therapy in the treatment of several solid tumors, OV patients only partially benefit from immune checkpoint blockade. Therefore, a biomarker is necessary to predict the responsiveness of OV patients to immunotherapy. This study sought to identify an immune-associated lncRNA-based prognostic signature to predict immunotherapy efficacy and chemosensitivity in OV patients.

Material and methods: We used ovarian cancer transcriptional profiles of patients from TCGA and GTEx databases with immune-related signature genes to screen immune-related lncRNAs. Furthermore, we integrated the GEO database to evaluate an immune-related lncRNA prognostic score (IRLRPI), and then verified the model in all aspects to distinguish biomarkers of IRLRPI subtypes.

Results: Our findings demonstrated that patients with elevated IRLRPI scores had a poorer prognosis and tended to be more immunosuppressed; in terms of treatment, these patients may exhibit resistance to immunotherapy and be less sensitive to several chemotherapeutic agents. Finally, the biomarkers KIF26B and VSTM2L were found to distinguish IRLRPI type.

Conclusions: The IRLRPI model we developed can predict immunotherapy responsiveness and chemotherapy sensitivity in ovarian cancer patients and demonstrates potential for clinical application.

Key words: ovarian cancer, lncRNAs, IRLRPI, immunotherapy, prognosis.

Introduction

Ovarian cancer is a highly lethal malignancy, with most patients diagnosed at an advanced stage, leading to a 5-year survival rate below 45% [1, 2]. Despite initial treatment with surgery and chemotherapy, the majority of patients develop chemoresistance and face recurrence

within a few years, highlighting a critical need for improved therapeutic strategies.

Despite the efficacy of immune checkpoint inhibitors (ICIs) in multiple solid tumors, their response rates in ovarian cancer remain dismal [3–5]. It is largely due to the high heterogeneity of ovarian cancer, which manifests in diverse tumor immune infiltration, metastatic potential, and treatment response. This underscores the imperative for predictive biomarkers. Immune-related gene prognostic scores (IRGPI) have emerged as a powerful tool for this purpose. In cancers such as head and neck squamous cell carcinoma (HNSCC), hepatocellular carcinoma, and esophageal carcinoma, low IRGPI scores are associated with favorable immune contexts (e.g., high CD8+ T cell infiltration) and predict superior ICI response [6–8]. Constructing such models via Cox regression represents a clinically convenient and highly predictive approach.

In recent years, the role of long non-coding RNAs (lncRNAs) in cancer has been increasingly elucidated. Accumulating evidence indicates that dysregulated lncRNA expression is closely implicated in tumor initiation and progression [9–11], establishing them as promising diagnostic biomarkers [12]. Furthermore, their potential as therapeutic targets underscores significant clinical value [13, 14]. Additionally, numerous studies have revealed that lncRNAs are pivotal regulators of the tumor immune microenvironment [15–17]. Emerging evidence indicates that immune-associated lncRNAs modulate tumor microenvironment composition and PD-1 blockade efficacy across multiple malignancies [18]. Therefore, multiple investigations employ immune-associated lncRNAs (IRlncRNAs) to develop prognostic signatures that predict immunotherapy efficacy across diverse cancers [19–21]. Previously, IRGPI and IRlncRNA-related models have been built for predicting the drug sensitivity, immune cell infiltration, and prognosis of clinical patients with OV [22, 23]. However, no existing models have been used for patients' immunotherapeutic response to OV.

By integrating TCGA and GTEX data, we established an IRlncRNA-based prognostic score (IRLRPI) for ovarian cancer. This model, trained in TCGA and validated in GEO, effectively stratified patients into high- and low-risk subgroups with distinct clinical outcomes, tumor immune microenvironments, and therapeutic responses. Two biomarkers, KIF26B and VSTM2L, were identified to aid in IRLRPI subtyping and prognosis assessment. The results showed that the IRLRPI score developed in this study provides a predictive indicator for immunotherapy and is also instrumental in identifying susceptible drugs for ovarian cancer patients.

Material and methods

Patients and data sources

In this study, 376 ovarian cancer samples from TCGA (https://portal.gdc.cancer.gov/) were selected to obtain gene expression data, clinical information, and single nucleotide mutation data. Transcriptome data of 88 normal ovarian tissue samples were downloaded from Genotype Tissue Expression (GTEx) (www.gtexportal.org/). Clinical and transcriptome data for GSE9891 were sourced from GEO (https://www.ncbi.nlm.nih.gov/geo/). Ensembl GTF annotations (http://asia.ensembl.org) enabled mRNA-lncRNA classification. Immune-related genes were curated from ImmPort (https://www.immport.org/) and InnateDB (https://www.innatedb.com/).

Construction of prognosis-related differentially expressed IRlncRNA sets

To analyze the correlation between immune-related genes and lncRNAs, we identified immune-related lncRNAs (IRlncRNAs) using |Pearson R| > 0.4 and $p < 0.001$ thresholds. The limma package in R software (https://www.r-project.org/) was used to analyze differences in the expression of IRlncRNA between tumor and normal tissue samples. Differentially expressed IRlncRNAs (DEIRlncRNAs) were identified using the criteria of log2FC (fold change) ≥ 2 and a false discovery rate (FDR) < 0.05. Next, the obtained DEIRlncRNA sets were normalized to the expression data from the GEO cohort. Finally, the overall survival was calculated using Kaplan-Meier survival analysis and log-rank tests. DEIRlncRNAs with significant effects on overall survival were screened to construct the prognosis-related DEIRlncRNA set.

Construction and verification of the IRLRPI

The IRLRPI was developed via multivariate Cox regression of prognosis-linked DEIRlncRNAs. For each sample, the index was computed as the sum of specific lncRNAs' expression values multiplied by their Cox regression coefficients. The formula of IRLRPI was as follows: IRLRPI = (–0.4243 × LEMD1-AS1 expression) + (0.1681 × LINC01127 expression) + (–0.2439 × TLR8-AS1 expression) + (–0.4590 × TYMSOS expression) + (0.9881 × LINC00452 expression) + (0.9418 × CACNA1G-AS1 expression) + (0.4219 × LINC00702 expression) + (–1.2146 × LINC00996 expression). The IRLRPI high/low-risk threshold corresponded to the cohort's median score. Consequently, the cut-off value is 1.

Kaplan-Meier/log-rank analyses assessed the IRLRPI's prognostic power in TCGA and GEO cohorts. To validate its independent prognostic value, ROC curves and univariate/multivariate Cox

regression were conducted using R packages (survival, survivalROC, survminer).

A prognostic nomogram was subsequently constructed using the R packages survival, regplot, and rms.

Analysis of tumor immune microenvironment

To characterize immune microenvironment variations across IRLRPI subtypes, we employed CIBERSORT to quantify the immune cell infiltration in the tumor microenvironment (TME) of patients. Then, we compared immune cell infiltration, immune activity, and checkpoint molecule expression between risk groups using R packages. Immune cells were tested using the Pearson correlation test, where $p < 0.05$ is shown in box plots, and results for immune response and checkpoint expression are displayed in box plots using the Wilcoxon rank sum test.

Immunotherapy responsiveness prediction

We downloaded immunophenoscores (IPS) of TCGA ovarian cancer patients from the TCIA database (https://tcia.at/) [24]. To anticipate immunotherapy response, IPS values were compared between IRLRPI subtypes using Wilcoxon rank-sum testing. We then obtained acquired transcriptomic data and clinical metadata for the phase II immunotherapy cohort (IMvigor210: http://research-pub.gene.com/IMvigor210CoreBiologies/) [25] and preprocessed the data using the authors' R package IMvigor210CoreBiologies. Patients in the cohort were scored for IRLRPI, and the predictive effect of different IRLRPI subtypes on immunotherapy response was observed [26].

Analysis of tumor mutation burden in different IRGPI subgroups

We calculated tumor mutation burden (TMB, number of mutations per 1Mb) for ovarian cancer patients using TCGA-derived SNP data. We profiled mutation landscapes across IRLRPI subtypes with the R package mafTools. We assessed TMB disparities between high- and low-risk groups via the χ^2 test [27].

Analysis of chemotherapy sensitivity in different IRGPI subgroups

We analyzed platinum, paclitaxel, PARP inhibitors, and other drugs commonly used in the TCGA ovarian cancer cohort ($n = 376$). Wilcoxon testing was used to assess differences in half-maximal inhibitory concentration (IC_{50}) between risk-stratified groups. The main R package used in this process was pRRophetic [28].

Unsupervised clustering

Consensus clustering was conducted via Consensus Cluster Plus with K-means [29], executing 100 iterations at 80% TCGA sample resampling. The cumulative distribution function (CDF) curve of consensus scores identified three optimal clusters.

IRLRPI-related biomarker screening

In the signal pathway analysis, the differentially expressed genes (DEGs) between IRLRPI risk groups ($|\log2FC| \geq 2$, FDR < 0.05) underwent gene set enrichment analysis (GSEA) using KEGG pathways ($p < 0.05$, FDR < 0.25), followed by functional annotation via GO enrichment.

Subsequently, LASSO (least absolute shrinkage and selection operator) [30] regression and SVM-REF (support vector machine–recursive feature elimination) [31] analysis were performed on all DEGs to screen for markers associated with IRLRPI typing. After the intersection of the genes obtained by the two machine learning methods, the differential gene expression in tumor versus normal tissues was analyzed via GEPIA (http://gepia.cancer-pku.cn/) [32]. The effects of these genes on OS were evaluated using K-M Plotter (http://kmplot.com) [33]. Finally, protein expression profiles in human tissues were evaluated by immunohistochemistry (IHC) using the Human Protein Atlas [34]. Following the above steps, the best quality biomarkers were finally selected from all genes obtained by machine learning.

Quantitative RT-PCR (QRT-PCR)

We obtained 15 ovarian cancer and 15 unpaired adjacent tissue from Shanghai Tenth People's Hospital. Following the manufacturer's guidelines, total RNA was extracted from tissues with TRIzol reagent (Takara, Japan). Reverse transcription was performed using the PrimeScript RT Master Mix kit (TaKaRa, Japan) and random primers. Real-time qPCR was performed following the supplier's instructions, with GAPDH acting as the endogenous control. The relative RNA expression was calculated using the $2^{-\Delta\Delta CT}$ method. Sequences of primers used in this study were as follows:

Forward (VSTM2L): 5′-CAGTGGTGGTATGTACGGAGC-3′;

Reverse (VSTM2L): 5′-CCTGCTTGTCGGTCCAGTC-3′;

Forward (KIF26B): 5′-GCTGGGAATAAAGAGAGGCTTG-3′;

Reverse (KIF26B): 5′-ACTCCTCGTATGCTTTCCGGT-3′;

Forward (GAPDH): 5′-GAAGGTGAAGGTCGGAGTC-3′;

Reverse (GAPDH): 5′-GAAGATGGTGATGGGATTTC -3′.

Statistical analysis

The independent prognostic value of the IRLRPI was evaluated using ROC curve analysis and univariate and multivariate Cox regression analyses, which were performed with the R packages survival, survival ROC, and survminer. Moreover, multivariable Cox regression modeling assessed survival outcomes as detailed in the Methods section.

A two-sided threshold of $p < 0.05$ was applied for significance.

Age was grouped as < 65 and ≥ 65 years. Staging was performed according to the FIGO staging system. Pathological diagnosis, tumor grade, and survival data were directly downloaded from TCGA (https://portal.gdc.cancer.gov/). The R package limma quantified differential immune features (cellular infiltration, functional responses, checkpoint markers) across IRLRPI risk strata. Immune cells were tested using the Pearson correlation test, where $p < 0.05$ is shown in box plots, and results for immune response and checkpoint expression are displayed in box plots, using the Wilcoxon rank sum test. The QRT-PCR results were compared using the unpaired *t*-test.

Results

Correlation between lncRNAs and prognosis in ovarian cancer

To determine whether lncRNAs regulate immune responses, 2935 immune genes and 2069 IRlncRNAs were selected from 13427 lncRNAs based on correlation analysis with the 2935 immune genes. We compared 376 ovarian cancer specimens and 88 normal specimens to obtain 1134 differentially expressed IRlncRNAs (Figure 1 A), of which 761 and 373 genes exhibited upregulation and downregulation, respectively, in OV (Figure 1 B). Through standardization and survival analysis, we selected 15 prognostic DEIRlncRNAs (Figure 1 C). Finally, for Cox regression analysis, the TCGA and GEO cohorts served as retrospective training and validation sets, respectively. As a result, eight lncRNAs were identified: LEMD1-AS1, LINC01127, TLR8-AS1, TYMSOS, LINC00452, ACNA1G-AS1, LINC00702, and LINC00996. These were used to construct an immuno-related lncRNA prognostic index (IRLRPI). Subsequently, we conducted univariate and multivariate Cox proportional hazards regression to assess the IRLRPI's prognostic utility. We found that IRLRPI served as an independent prognostic factor for patients (Figures 1 D, E), and the predictive effect of IRLRPI was stable over time (Figures 1 F, G). The overall survival of the two IRLRPI subtypes also showed significant differences. Patients with high IRLRPI scores exhibited poorer overall survival, while those with low IRLRPI scores showed improved prognosis (Figures 1 H, I). Regarding clinical staging, a greater proportion of patients in the high-IRLRPI group were classified as advanced stage compared with those in the low-IRLRPI group (Supplementary Figure S1). Finally, to further improve the diagnostic efficiency of IRLRPI, we added age, clinical stage, and case grading to construct a nomogram (Supplementary Figure S2 A), and the nomogram was used to repredict the prognosis of the patients (Supplementary Figure S2 B). The nomogram facilitates clinical translation of the prognostic model. Thus, we identified a significant association between IRLRPI and ovarian cancer prognosis via the nomogram.

Relationship between IRLRPI and immune infiltration to predict immunotherapy in ovarian cancer

Since immune-related lncRNAs underpin IRLRPI construction, we investigated associations between IRLRPI subtypes and immune cell infiltration as well as biological functions in ovarian cancer. Tumor samples were categorized into high- and low-risk subtypes according to IRLRPI expression levels. First, we analyzed the immune infiltrated cells in the tumor microenvironment (TME) between two IRLRPI subtypes. We found that most immune cells were negatively correlated with scores, while tumor-associated fibroblasts and regulatory T cells (Treg) were positively correlated (Figure 2 A). Interestingly, differences in immune responses and immunophenotyping were observed between the two IRLRPI subtypes: the immune scores of inflammations promoting HLA, MHC class I, and type I IFN response were significantly lower in the high-IRLRPI group, while type II IFN response was significantly activated (Figure 2 B); in immunophenotyping, patients with high IRLRPI scores predominantly exhibited a wound healing phenotype, whereas those with low IRLRPI scores were mostly IFN-γ-dominant (Supplementary Figure S3).

Subsequently, we profiled immune checkpoint gene expression across IRLRPI subtypes. We found that immunotherapy-related targets with significant differences all showed low expression in high-IRLRPI subtypes, including the commonly used immune checkpoint blocker targets PDCD1, CD274, and CTLA4, which may predict that the immunotherapy sensitivity in the high-IRLRPI subtype may be lower ($p < 0.05$) (Figure 2 C). Our IPS scoring of immune response in ovarian cancer patients further validated this conclusion using TCIA ($p < 0.05$) (Figure 2 D). We leveraged the landmark IMvigor210 immunotherapy cohort to validate the IRLRPI's predictive capacity for immunotherapy response. The results revealed that the high-IRLRPI subtype had lower CR/PR rates ($p = 0.013$) after immunotherapy, with poor prognosis ($p < 0.001$)

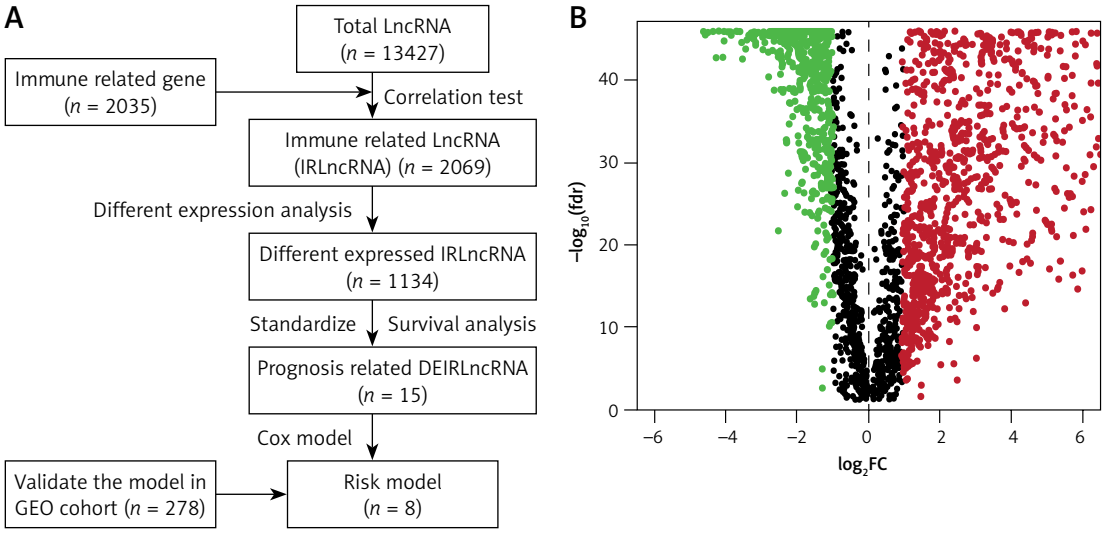

C

	P-value	Hazard ratio
LEMD1-AS1	0.026	0.764 (0.603–0.968)
LINC01127	0.047	1.165 (1.002–1.355)
USP30-AS1	0.002	0.636 (0.476–0.851)
DLG3-AS1	0.040	0.704 (0.503–0.984)
DEPDC1-AS1	0.031	0.498 (0.264-0.936)
UBXN10-AS1	0.008	0.709 (0.549–0.916)
TLR8-AS1	0.026	0.769 (0.610–0.970)
TYMSOS	< 0.001	0.570 (0.415-0.782)
NDUFB2-AS1	0.046	0.618 (0.385–0.991)
ZFHX4-AS1	0.007	1.763 (1.170–2.657)
LINC00452	0.035	2.081 (1.051–4.118)
CACNA1G-AS1	< 0.001	2.998 (1.592–5.647)
LINC01231	0.031	0.687 (0.488-0.966)
LINC00702	0.041	1.737 (1.024-2.945)
LINC00996	0.003	0.337 (0.166-0.685)

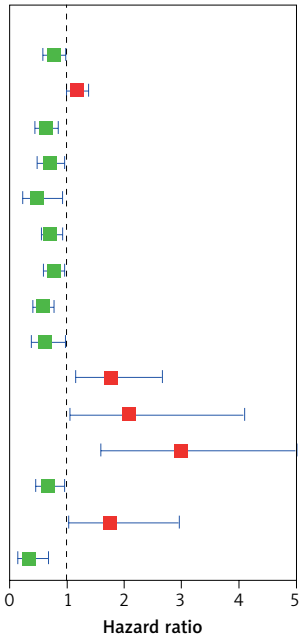

D

	P-value	Hazard ratio
Age	< 0.01	1.023 (1.010–1.038)
Stage	0.068	1.312 (0.980–1.755)
Grade	0.372	1.202 (0.803–1.798)
RiskScore	< 0.001	1.601 (1.435–1.786)

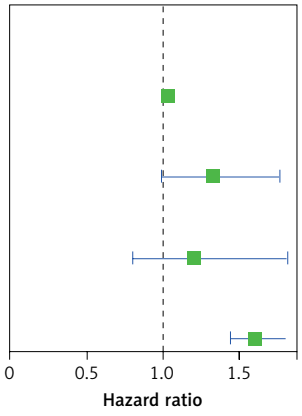

Figure 1. Construction and predictive effect assessment of IRLRPI. **A** – Screening process of lncRNAs used for model construction. **B** – Volcano map of lncRNAs differentially expressed in ovarian cancer and normal tissues. **C** – Forest plot of lncRNA risk associated with prognosis of ovarian cancer patients. **D** – Univariate and multivariate Cox (**E**) analysis for assessing the effect of IRLRPI

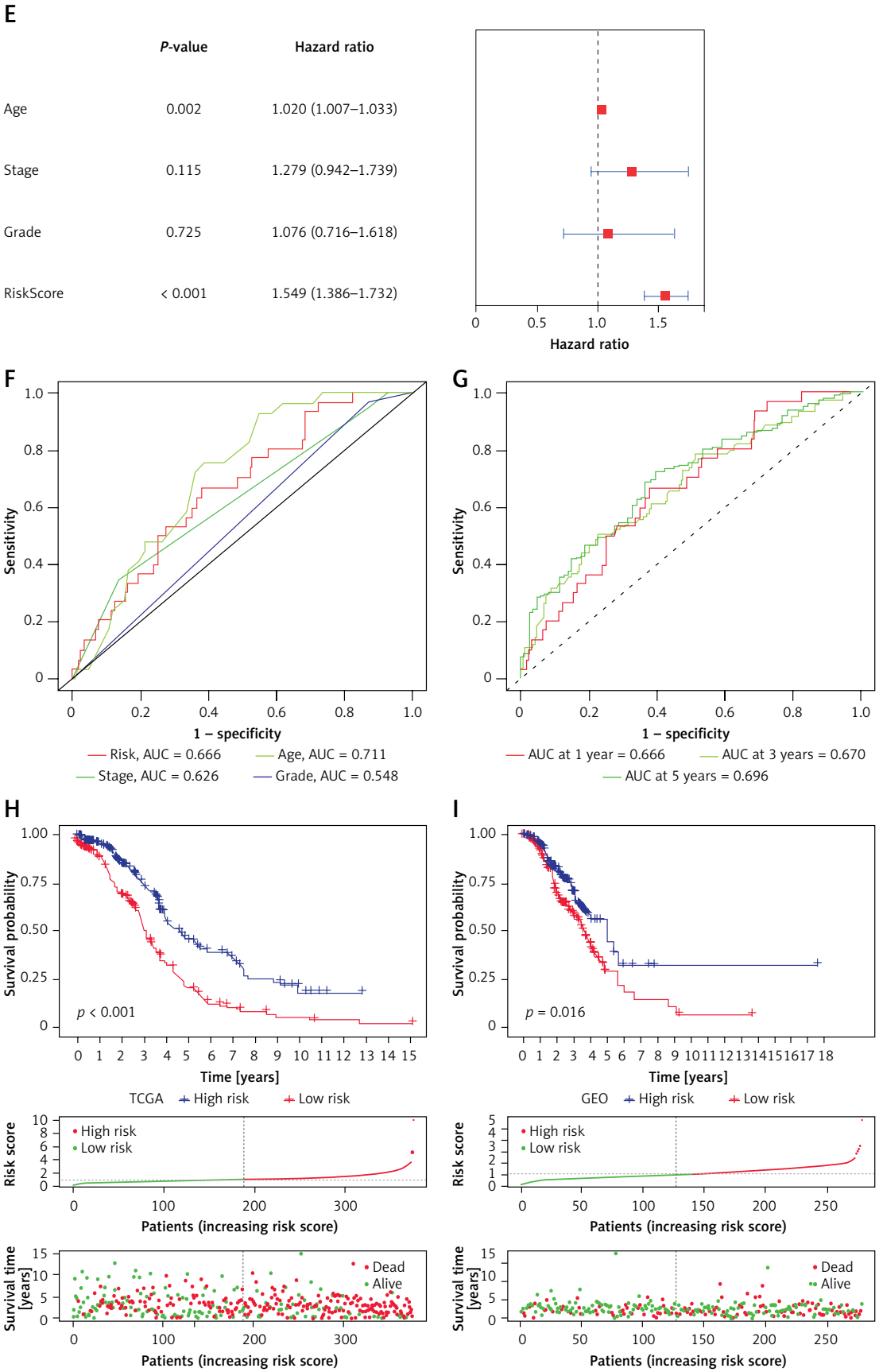

Figure 1. Cont. **D** – Univariate and multivariate Cox (**E**) analysis for assessing the effect of IRLRPI. **F** – ROC analysis of age, stage, grade, and IRLRPI. **G** – ROC analysis of 1-year, 3-year, and 5-year IRLRPI. **H** – Survival analysis of high and low IRLRPI in TCGA cohort, IRLRPI thresholds and scatter plots of IRLRPI versus patient survival. **I** – Survival analysis of high and low IRLRPI in GSE9891, IRLRPI thresholds, and scatter plots of IRLRPI versus patient survival

(Figure 2 E). These results demonstrate the IRLRPI's strong potential as a predictor of immunotherapy response in patients.

Analysis of TMB and chemotherapy drug sensitivity according to IRLRPI

The tumor mutation burden (TMB) and the efficacy of immunotherapy were closely correlated [35, 36]. Thus, we compared TMB profiles between IRLRPI subtypes (Figure 3 A), observing no significant difference. Subsequent survival analysis revealed improved prognosis in patients with elevated TMB (Figure 3 B). Patients had the best overall survival when they were also in the low-IRLRPI group, and vice versa (Figure 3 C). Therefore, it is suggested that TMB be added as

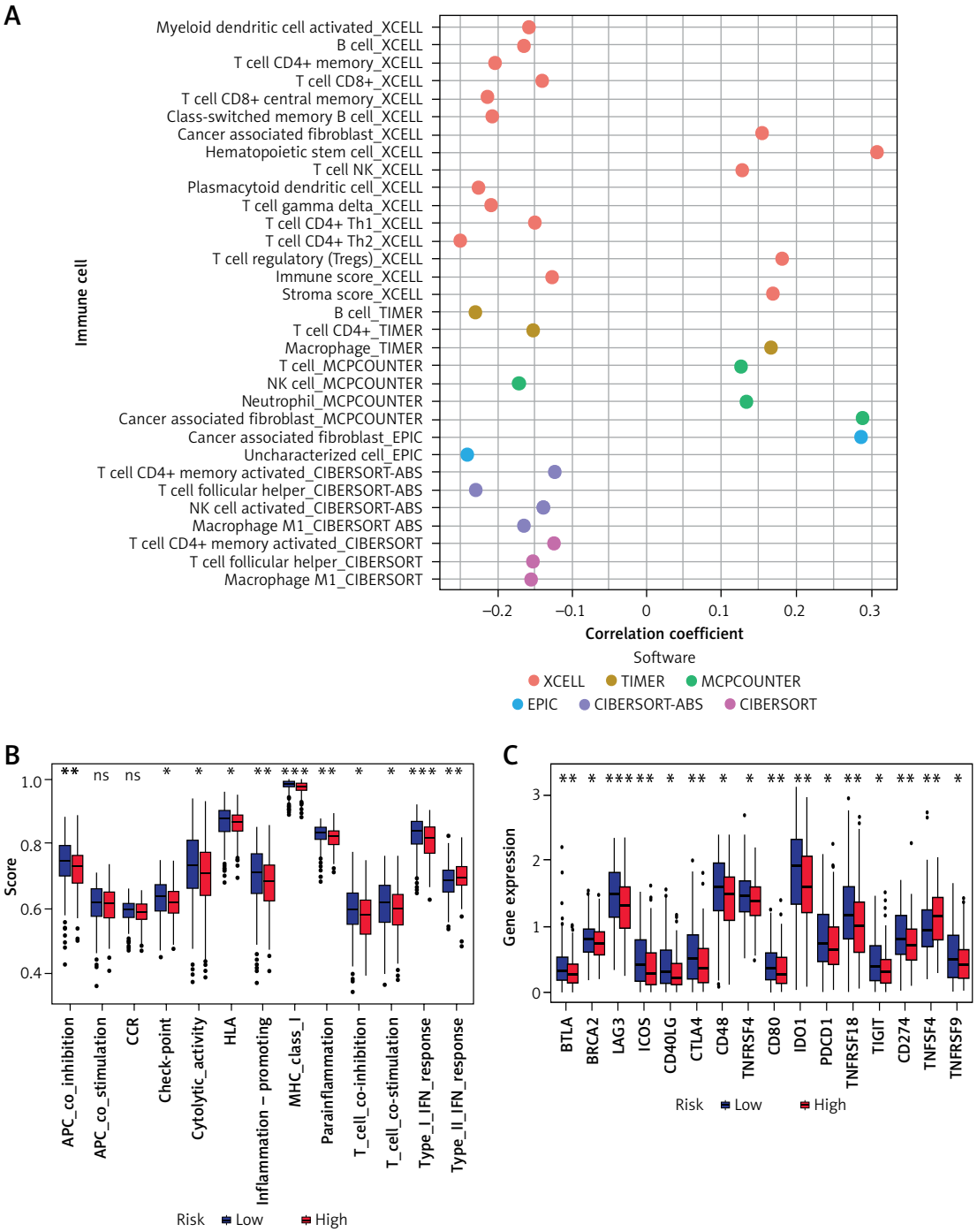

Figure 2. Relationship between IRLRPI and immune infiltration and immunotherapy. **A** – Dot plot of correlation between IRLRPI and immune cell infiltration ($p < 0.05$, correlation coefficient > 0.1). **B** – Box plot of gene expression differences in immune function and immune checkpoint (**C**) between IRLRPI subgroups (ns, $p > 0.05$, *$p < 0.05$, **$p < 0.01$, ***$p < 0.001$)

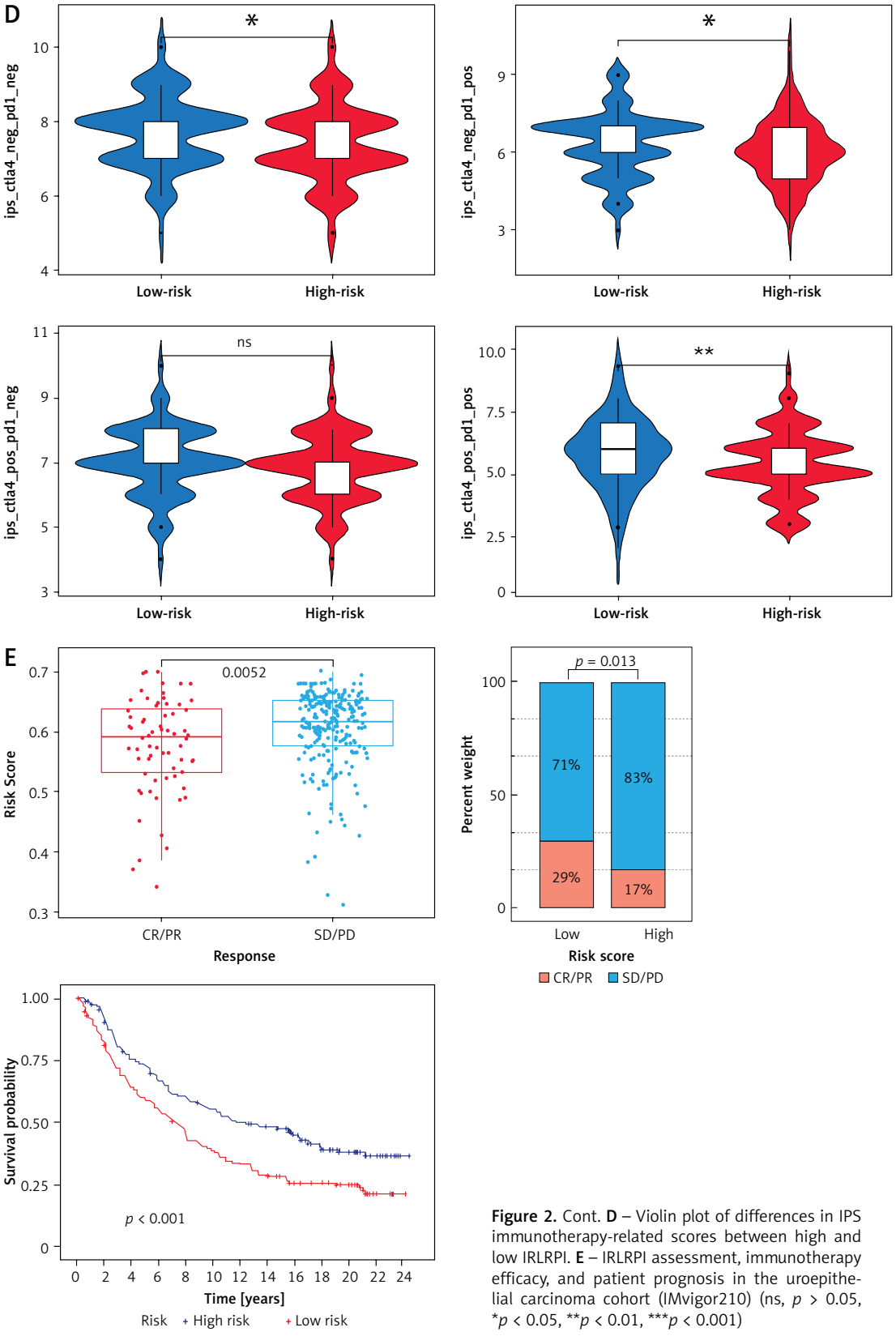

Figure 2. Cont. **D** – Violin plot of differences in IPS immunotherapy-related scores between high and low IRLRPI. **E** – IRLRPI assessment, immunotherapy efficacy, and patient prognosis in the uroepithelial carcinoma cohort (IMvigor210) (ns, $p > 0.05$, *$p < 0.05$, **$p < 0.01$, ***$p < 0.001$)

a relevant index in practical clinical applications to provide a more accurate prediction of patient prognosis. We systematically evaluated chemotherapy drug sensitivity profiles across IRLRPI subtypes, identifying statistically significant differential responses between these subgroups. Among them, the low-IRLRPI type was more sensitive to paclitaxel, PARP1 inhibitor (ABT.888), mitomycin C,

and methotrexate, while high-IRLRPI was more sensitive to tyrosine kinase inhibitor (pazopanib) (Figure 3 D). These drugs constitute standard-of-care regimens for ovarian cancer; therefore, the results could provide some advice and guidance on chemotherapy for both types of patients.

Consensus clustering is classified according to IRLRPI in OV patients

To better characterize the type of patients with ovarian cancer, we performed consensus clustering of the two IRLRPI subgroups and obtained 3 clusters (Figure 4 A). Among them, cluster 1 (C1)

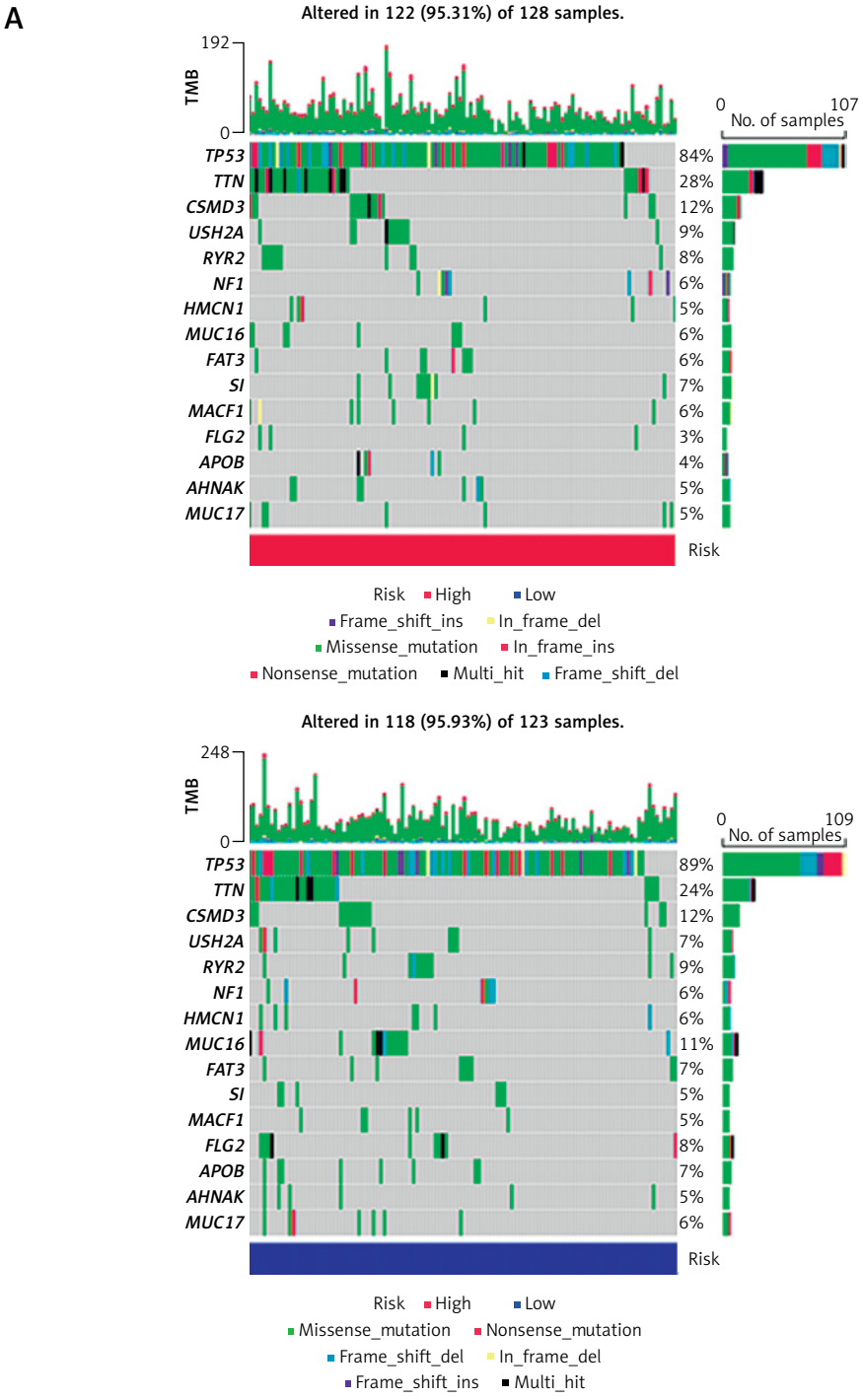

Figure 3. Correlation analysis between IRLRPI and TMB and chemotherapeutic drug sensitivity. **A** – Significantly mutated genes in ovarian cancer samples with mutations in different IRLRPI subgroups. Mutated genes (rows, top 10) are sorted by mutation rate; samples (columns) are arranged to emphasize reciprocity between mutations. The percentage of mutations is shown on the right, and the total number of mutations is shown at the top. Color coding indicates mutation type. **B** – Survival analysis of high and low tumor mutational load (TMB) in ovarian cancer patients

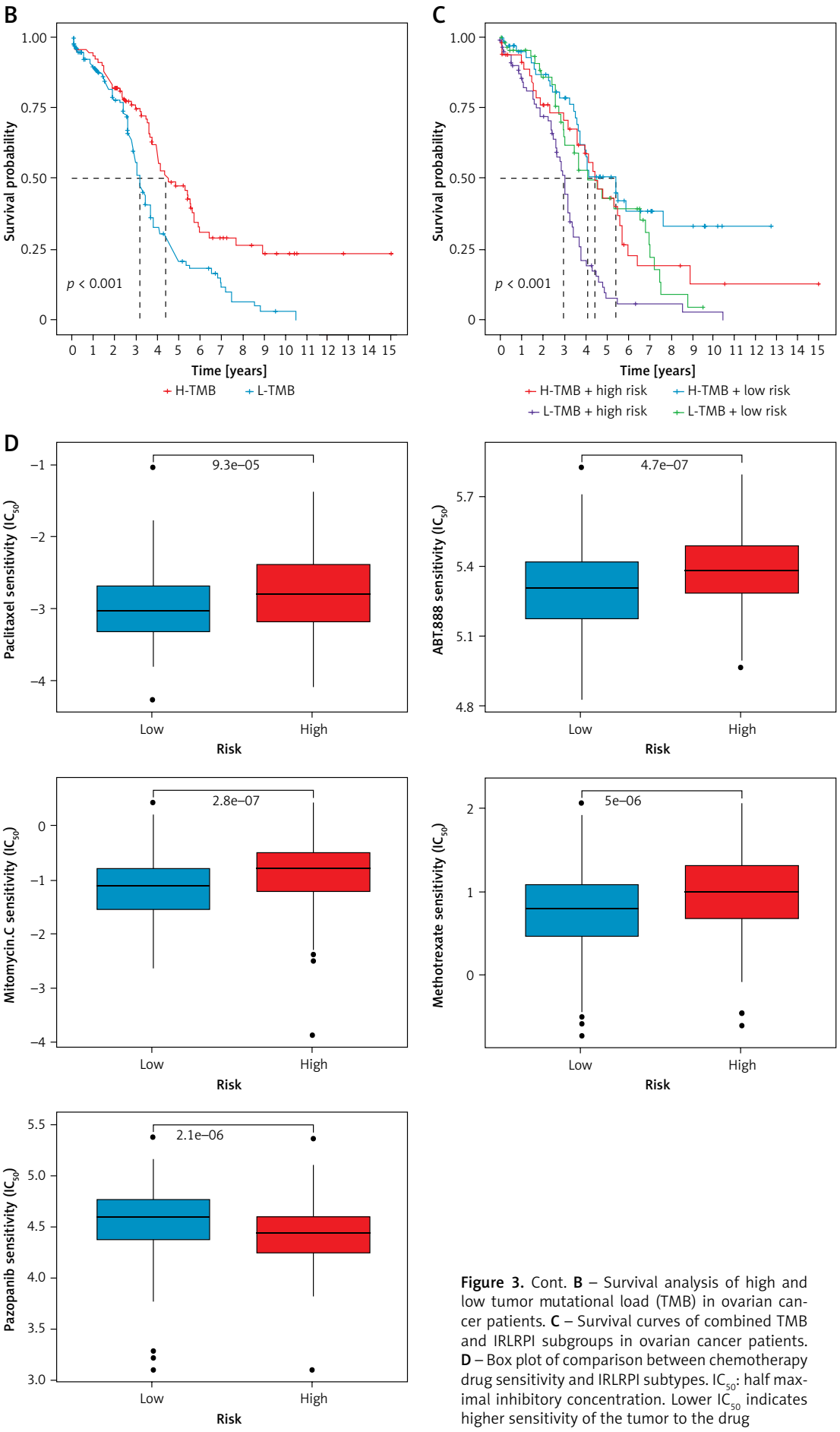

Figure 3. Cont. **B** – Survival analysis of high and low tumor mutational load (TMB) in ovarian cancer patients. **C** – Survival curves of combined TMB and IRLRPI subgroups in ovarian cancer patients. **D** – Box plot of comparison between chemotherapy drug sensitivity and IRLRPI subtypes. IC_{50}: half maximal inhibitory concentration. Lower IC_{50} indicates higher sensitivity of the tumor to the drug

had greater representation of patients in the high-IRLRPI subtype, cluster 2 (C2) had a higher proportion of patients in the low IRLRPI subtype, and cluster 3 (C3) was almost equally composed of patients in both subtypes (Figure 4 B). The survival analysis results were broadly consistent with the IRLRPI results, with C1, which had more high-IRLRPI subtypes, having the worst prognosis, and C2, which had the fewest high-IRLRPI subtypes, having a relatively good prognosis (Figure 4 C). Subsequently, we analyzed immune checkpoint gene expression across three clusters, identifying significantly differential PD-L1 (CD274) expression (Figure 4 D). We profiled immune cell infiltration across three clusters, revealing significant differences in select immune cell subsets: B cells, myeloid dendritic cells, and specific T cell subpopulations (Figure 4 E). Finally, we assessed chemotherapy sensitivity profiles across the three clusters, and we found that: C3 patients were the least sensitive to MEK inhibitor (AZD6244) but most sensitive to cisplatin and vincristine; and C2 patients were the most insensitive to tyrosine kinase inhibitor (pazopanib) (Figure 4 F). Through this unsupervised clustering method, patients could be divided into their IRLRPI subtypes, and the accuracy of the IRLRPI model was improved.

Screening for signature genes VSTM2L and KIF26B for IRLRPI typing using machine learning

To better understand the related functions of differentially expressed genes (DEGs) and screen out novel biomarkers suitable to assist in screening the IRLRPI subtypes, we obtained DEGs between IRLRPI subgroups (Figure 5 A). We performed a functional enrichment analysis of these genes. Among them, genes in the high-IRLRPI subtype were enriched in tumor proliferation (MAPK signaling pathway) and migration (ECM receptor interaction, focal adhesion) related pathways (Fig-

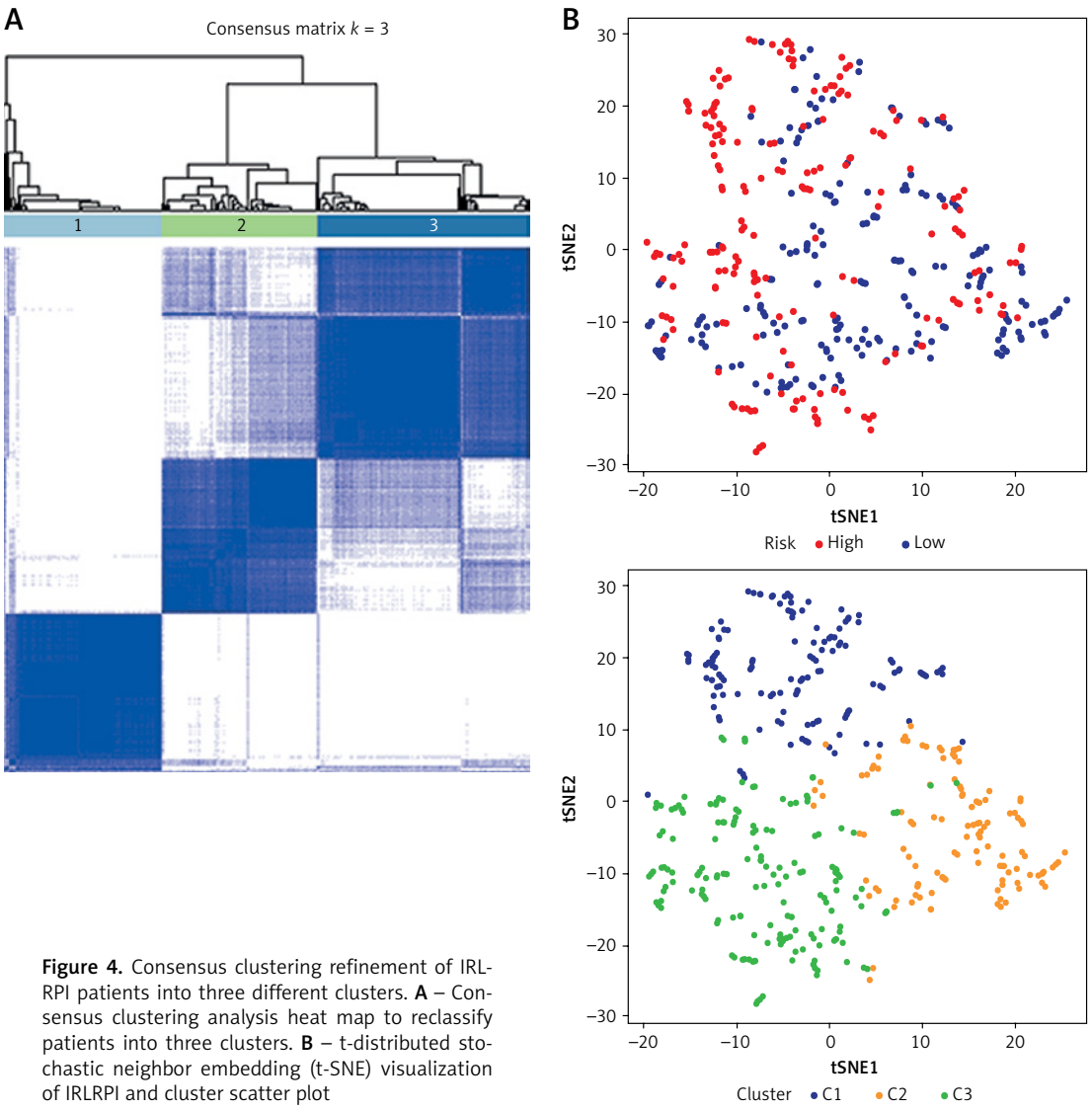

Figure 4. Consensus clustering refinement of IRLRPI patients into three different clusters. **A** – Consensus clustering analysis heat map to reclassify patients into three clusters. **B** – t-distributed stochastic neighbor embedding (t-SNE) visualization of IRLRPI and cluster scatter plot

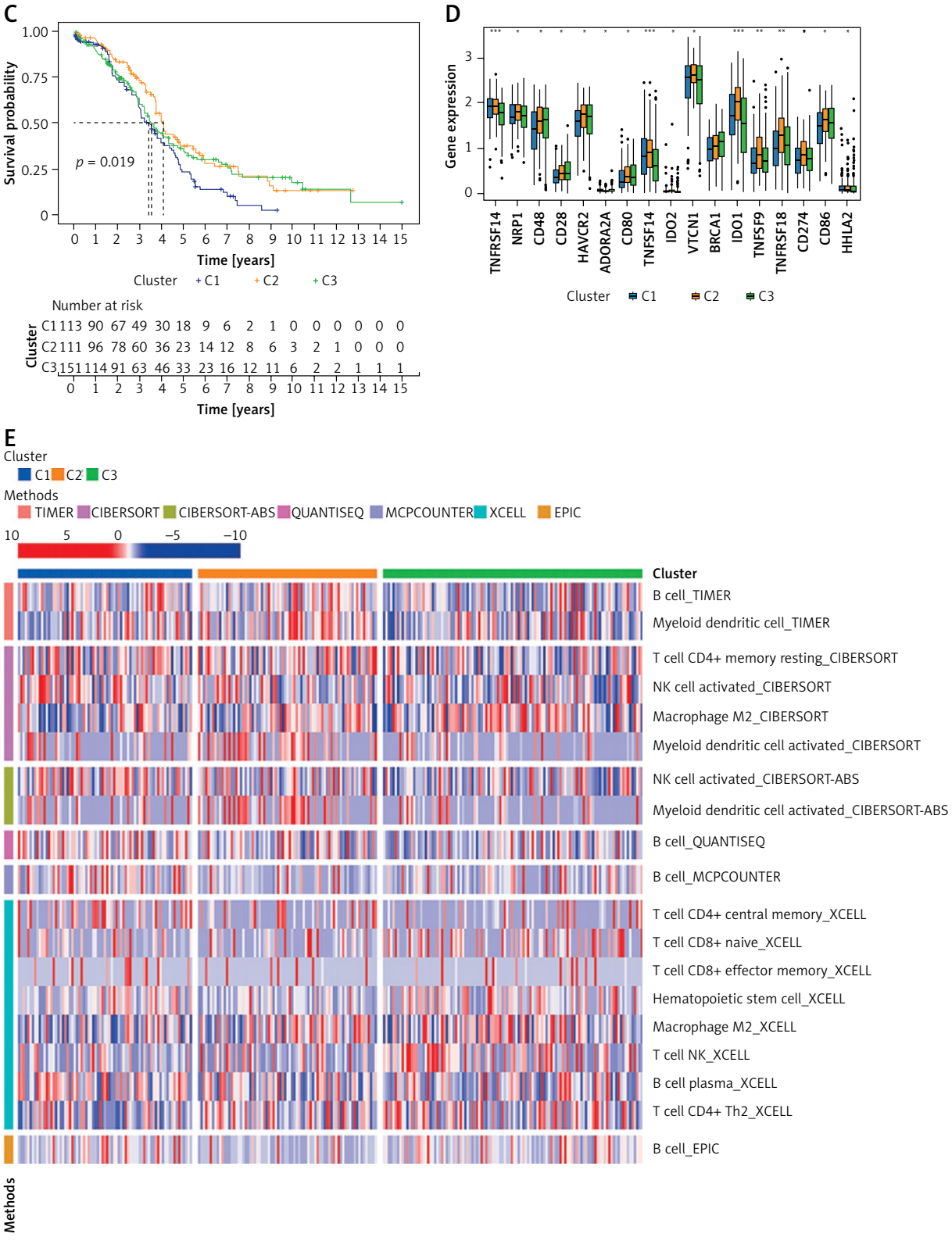

Figure 4. Cont. **C** – Survival curve plot for the three clusters. **D** – Box plot of the difference of immune checkpoint expression between the three clusters (*p < 0.05, **p < 0.01, ***p < 0.001). **E** – Heat map of cells with significant infiltration differences between the three clusters (p < 0.05)

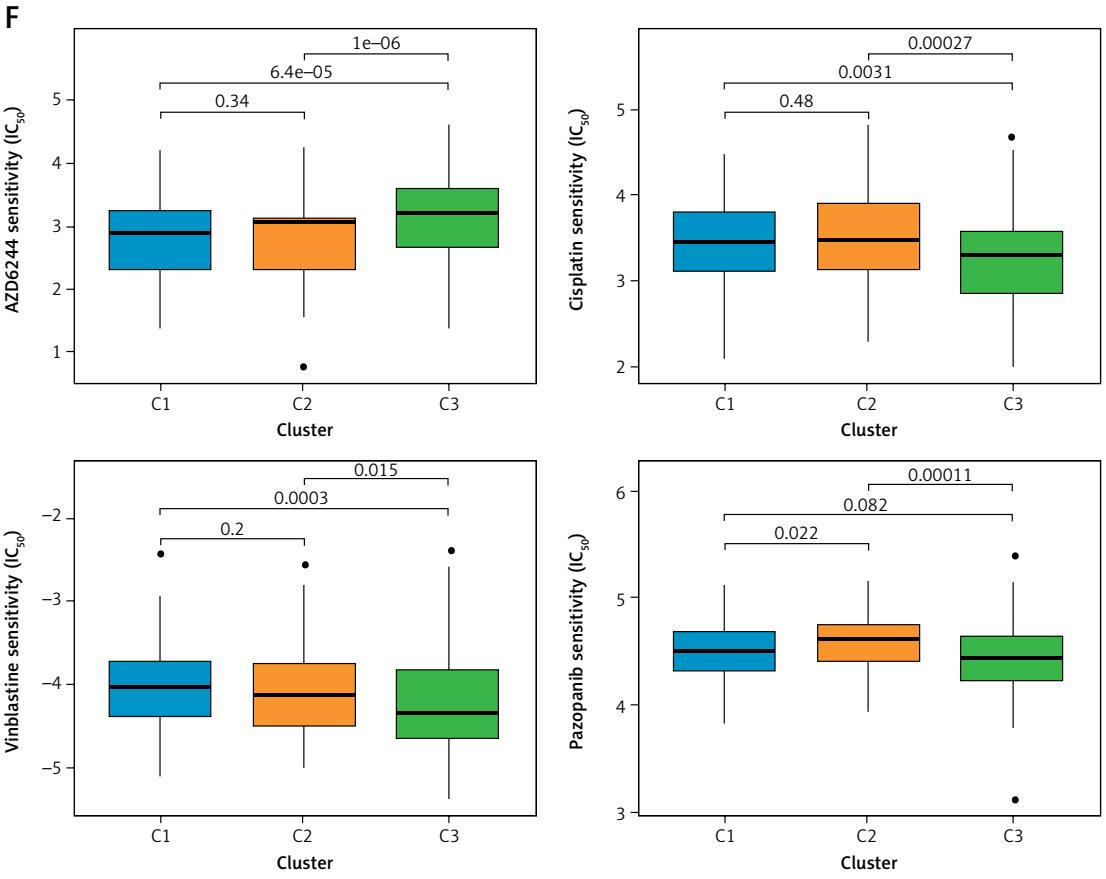

Figure 4. Cont. **F** – Box plot of chemotherapeutic drug sensitivity between the different clusters

ure 5 B). Conversely, low-risk patients exhibited significant enrichment in immune pathways: antigen processing/presentation, chemokine signaling, and primary immunodeficiency (Figure 5 C). Comprehensive GO analysis of all combined differential genes revealed significant enrichment in immune system processes and cell migration pathways (Figure 5 D). Next, to find the biomarkers associated with our IRLRPI model of DEGs, we first screened a total of 22 IRLRPI signature genes using lasso regression (Figure 5 E) and 34 IRLRPI signature genes using SVM-REF analysis (Figure 5 F). After taking the intersection of the signature genes obtained from the two machine learning approaches, 21 genes were identified as significantly associated with IRLRPI-based molecular subtyping (Supplementary Figure S4 A). We finally selected two genes, VSTM2L and KIF26B, as biomarkers of IRLRPI based on the expression of these genes and their impact on patient survival prognosis. Both genes exhibited marked upregulation in OV (Figures 5 G, H; Supplementary Figure S4 B, C). Also, high expression of both genes corresponded to a worse prognosis of patients (Figure 5 I; Supplementary Figure S4 D). Notably, VSTM2L expression positively correlated with clinical stage, exhibiting progressive upregulation in advanced ovarian cancer (Figure 5 J).

Finally, a total of 15 ovarian cancer tissue samples and 15 unpaired adjacent normal tissue samples were acquired from Shanghai Tenth People's Hospital. It was found that two marker genes exhibited significant upregulation in the ovarian cancer group (Figure 6 A). We also observed a positive correlation between IRLRPI scores and expression of two signature genes in TCGA ovarian cancer patients (Figure 6 B), as well as with the expression levels of the lncRNAs constituting the scoring system (Supplementary Figure S5 A, B). This further demonstrates the reliability of these two genes as auxiliary biomarkers for IRLRPI grouping.

Discussion

OV has the highest mortality rate among gynecologic tumors because of difficulties in diagnosis and chemotherapy resistance. Meanwhile, immunotherapy, which has achieved good results in other gynecologic tumors [37, 38], has been less effective in OV. Thus, there is an urgent demand to develop relevant markers for the early triage of patients. In the present work, we constructed an immune-related lncRNA prognostic index (IRLRPI) comprising eight lncRNAs from the TCGA ovarian cancer cohort, and then evaluated the predictive

efficiency of the IRLRPI in all aspects. Finally, we screened for biomarkers among DEGs associated with the typing of IRLRPI. This study comprehensively illustrated that our constructed IRLRPI model not only could predict the immunotherapeutic response, but also had greater clinical value than other established models.

Previous studies predominantly examined survival-associated immune lncRNAs in epithelial ovarian cancer (EOC). However, they were used as an independent predictive signature with significant prognostic value in ovarian carcinoma [22, 23, 39, 40]. Thus, these existing models have some limitations in clinical application. Significantly, lncRNAs comprising our model participate in ovarian carcinogenesis and progression. Reduced LEMD-AS1 expression correlates with poorer outcomes and diminished immune infil-

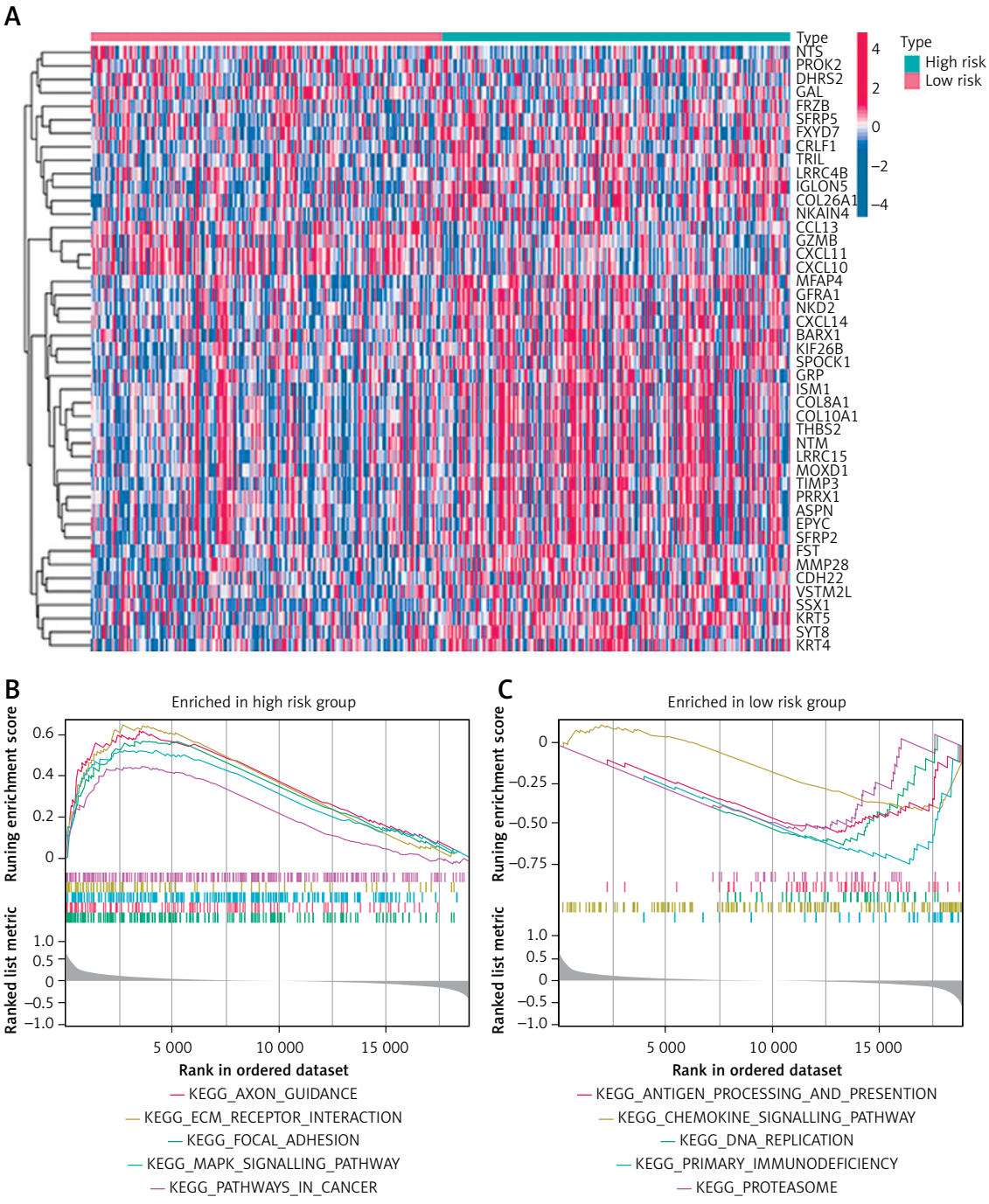

Figure 5. Signature genes between the two IRLRPI subtypes were screened based on machine learning. **A** – Heat map of differentially expressed genes between high- and low-IRLRPI groups. The heatmap is annotated with IRLRPI groupings (top bar) and gene expression levels (red for high, blue for low). Each vertical line (column) in the plot denotes a single patient. **B** – Gene set enrichment analysis plot for the high-IRLRPI group ($p < 0.05$, FDR < 0.25). **C** – Gene set enrichment analysis plot for the low-IRLRPI group ($p < 0.05$, FDR < 0.25)

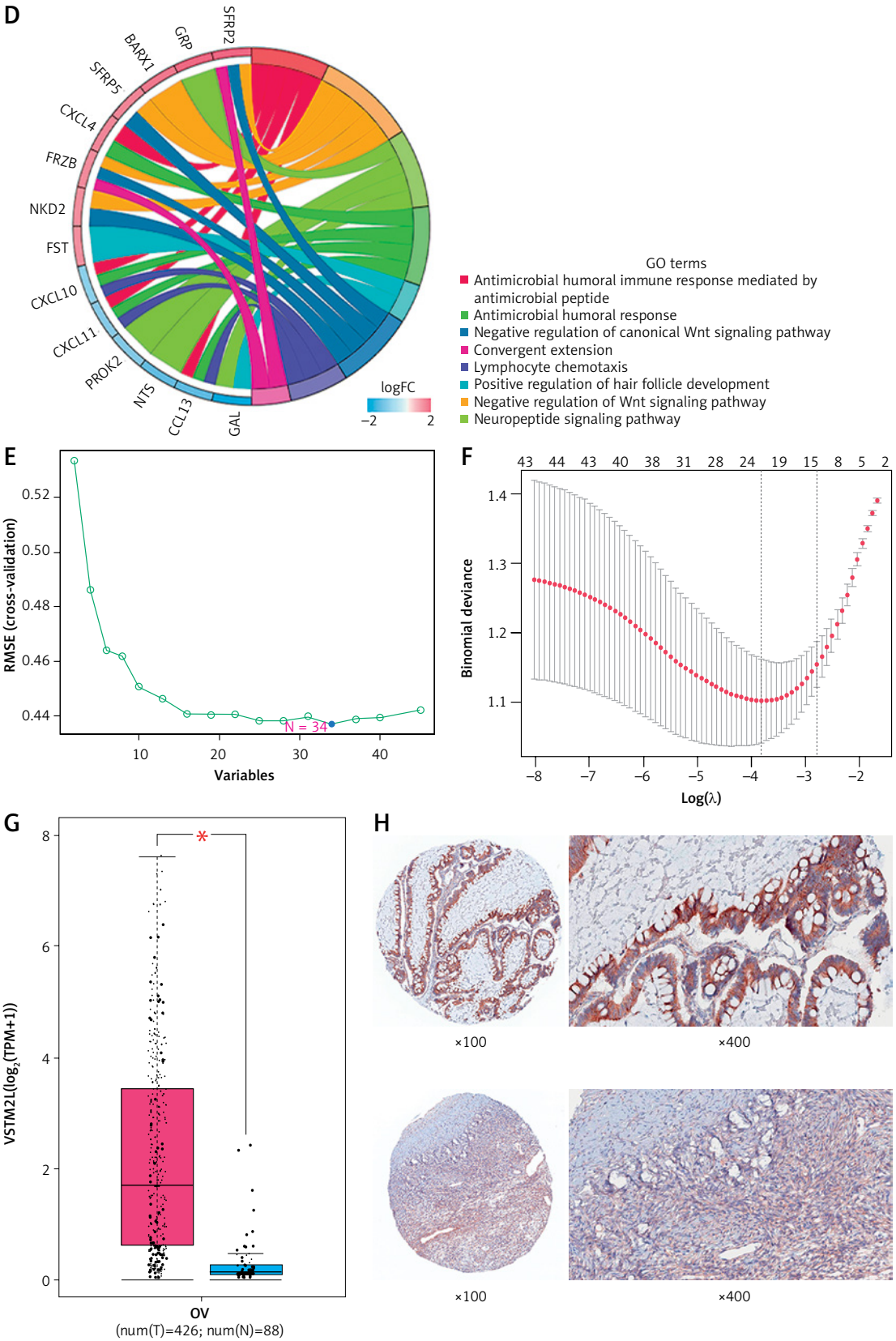

Figure 5. Cont. **D** – Gene Ontology enrichment analysis of total differential genes. The chord diagram illustrates the most significantly differentially expressed genes (left) between the two IRLRPI groups and their corresponding enriched pathways (right). **E** – Absolute shrinkage and selection operator regression screening for genes associated with IRLRPI grouping. **F** – Support vector machine–recursive feature elimination analyzing genes associated with IRLRPI grouping. **G** – Box plot of the difference in VSTM2L expression between normal and tumor tissues (log2 fold change > 1; $p < 0.05$). **H** – Pathological section of VSRM2L with TCGA ovarian cancer and GTEx normal ovaries in the HPA database

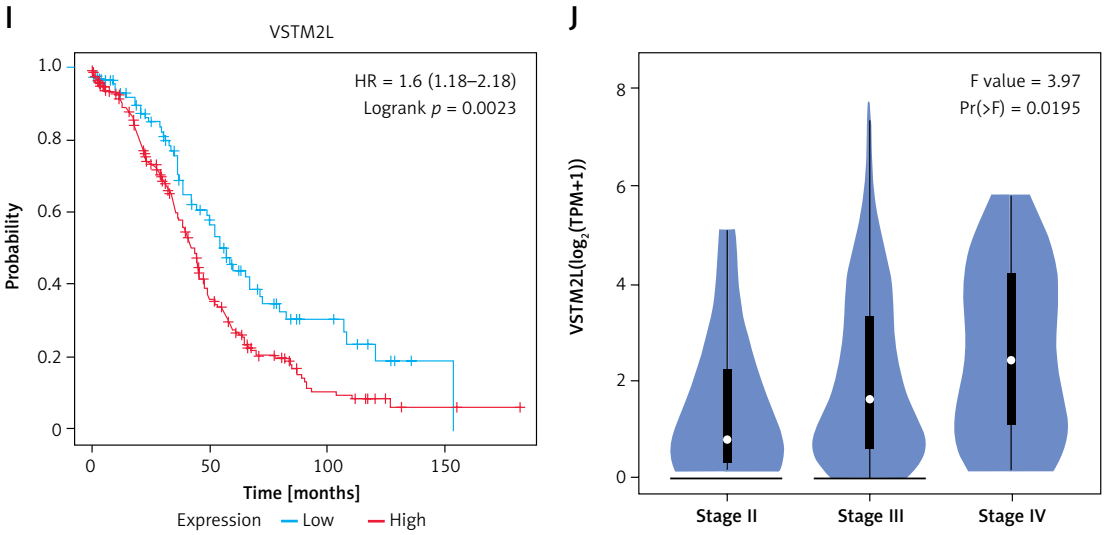

Figure 5. Cont. **I** – K-M curves of survival differences between high and low VSTM2L expression in ovarian cancer patients. **J** – Violin plot of the correlation between VSRM2L and patients' tumor stage

tration in patients [41]. LINC01127 was shown to regulate the cell cycle and promote the development of ovarian tumors [42]. TLR8-AS1 enhanced metastasis ability and chemoresistance in ovarian cancer [43]. LINC00452 drives ovarian oncogenesis via miR-501-3p sequestration and ROCK1 stabilization through impaired ubiquitin-mediated degradation [44]. LINC00702 promotes ovarian tumor progression by recruiting EZH2 to transcriptionally repress KLF2 [45]. However, TMYSOS, ACNA1G-AS1, and LINC00996 were not found to be involved in ovarian cancer-related biological functions. These studies involving the function of lncRNAs used in this model could partially explain why our model could predict patients' prognosis and treatment response. In subsequent results, we assessed the differences in the tumor microenvironment among different IRLRPI subtypes, which included tumor-infiltrating immune cells and stromal cells. Among tumor-infiltrating immune cells, the high-IRLRPI group exhibited lower T cell and macrophage infiltration, whereas Treg cell infiltration was elevated. Accumulating evidence has established robust correlations between diminished T-lymphocyte and macrophage infiltration [46], concomitant elevation in regulatory T-cell abundance [47], and inferior clinical responses to immunotherapeutic interventions [48, 49]. On the other hand, cancer-associated fibroblasts (CAFs) demonstrated the most pronounced stromal variation, exhibiting elevated abundance in high-IRLRPI subtypes. CAFs have been shown to enhance chemoresistance and promote cancer progression in ovarian cancer [50, 51]. Therefore, differences in immune infiltration may contribute to poor prognosis and insensitivity to chemotherapeutic agents in patients with the high-IRLRPI subtype.

Furthermore, we identified significant associations of IRLRPI with key immune processes and immune checkpoint gene expression profiles. The results suggested that antigen-presenting processes and type I interferon responses are significantly inhibited, but type II interferon responses are activated in the tumor microenvironment in high-risk patients. This paradox might be explained by their different roles in the immune process. Commonly, the type I interferon response has been shown to kill tumors [52, 53] and influence the efficacy of therapy [54]. As for type II interferon, recent research showed that it could suppress antitumor immune responses [55]. It might explain why the type II interferon responses are activated in high-risk subtypes. On the other hand, expression levels of immune checkpoint genes such as PD-1, CD274, and CTLA4 are generally significantly reduced in patients in the high-IRLRPI group [56]. All these results could explain the differences in immunotherapy response between IRLRPI subtypes.

To date, clinical evidence demonstrates limited efficacy of immunotherapy for OV whether alone or combined with chemotherapeutic agents [57–59]. For instance, the KEYNOTE-100 trial used immune checkpoint inhibitors in 376 patients and observed a very low overall remission rate (8.5%). Therefore, we hypothesize that IRLRPI is expected to have great potential in the prediction of immunotherapy effects. To verify the predictive performance of IRLRPI regarding immunotherapy response, we used IPS to predict patients' immunotherapy responses. The IPS scoring system exhibits strong predictive performance for anti-PD-1 and anti-CTLA-4 efficacy [24], with higher scores correlating to improved immunotherapy response. Reduced IPS scores in high-IRLRPI patients correlate with attenuated immunotherapy response.

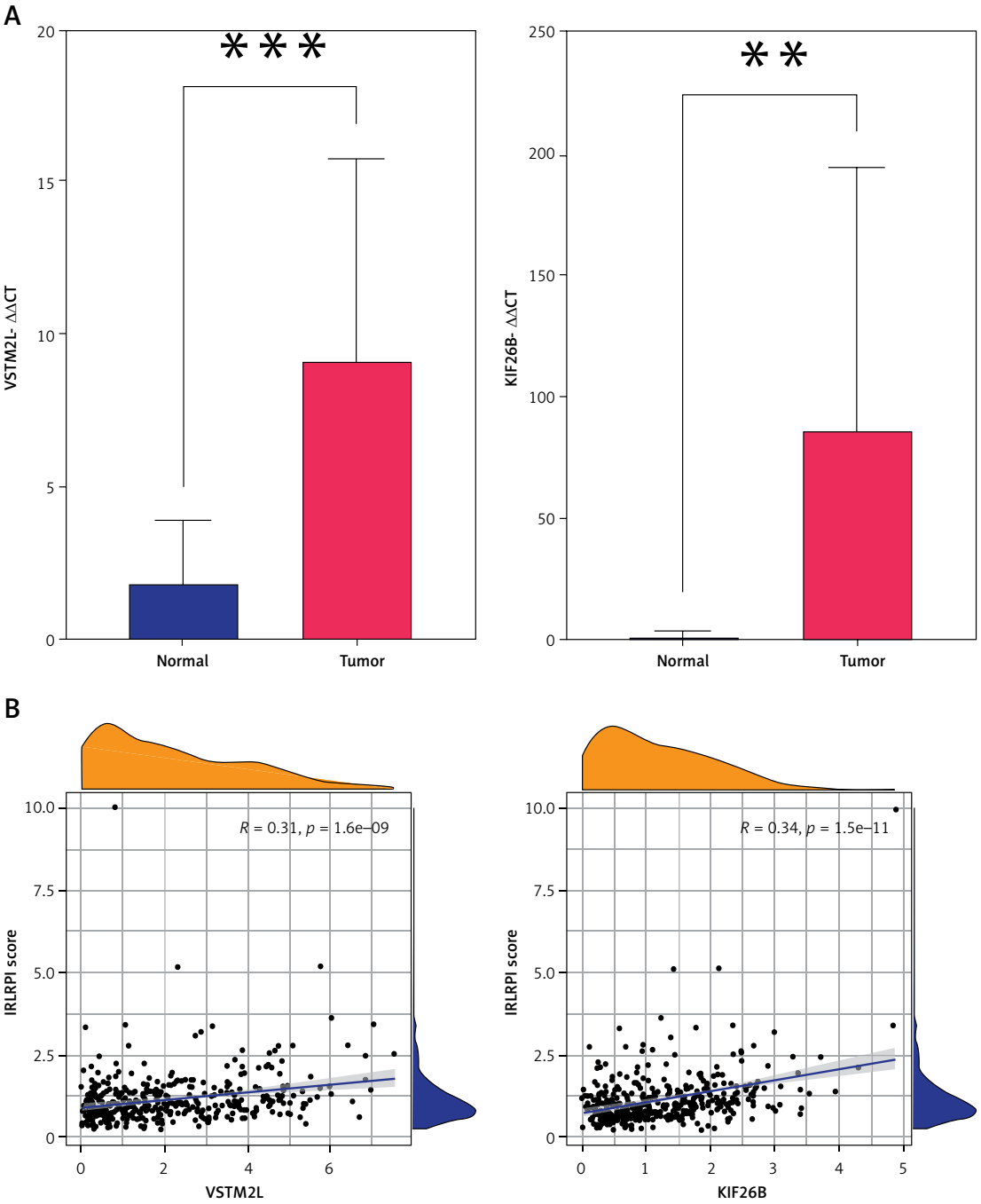

Figure 6. Tissue-specific expression patterns of the feature genes VSTM2L and KIF26B (**A**) and their correlations with patient IRLRPI scores (**B**)

We also used IMvigor210, a classic immunotherapy cohort for urothelial carcinoma, to externally verify the IRLRPI's prognostic utility for immunotherapy response [60–62]. High-IRLRPI patients demonstrated inferior immunotherapy responses and clinical outcomes. Collectively, these findings position the IRLRPI score as a novel biomarker capable of predicting immunotherapy response, thereby holding significant potential to guide and optimize therapeutic selection for patients with ovarian cancer.

Tumor mutation burden (TMB) closely correlates with tumor neoantigen load and critically mediates immune clearance of tumor cells through neoantigen recognition. Thus, TMB is considered associated with immunotherapeutic efficacy [35]. Our IRLRPI typing result was not significantly related to patients' TMB, probably because the establishment of our model may focus more on the immune infiltration and response rather than the amount of neoantigen in patients [63]. TMB is also an important adjunct to our model, and we

found that high-risk IRLRPI scores tend to be accompanied by lower TMB, which suggests that patients probably have worse treatment outcomes. In terms of chemotherapy response, we assessed patients' sensitivity to targeted chemotherapeutic agents using the metric IC_{50}. Paclitaxel, used in first-line chemotherapy for ovarian cancer, was insensitive in patients with the high-IRLRPI subtype. In contrast, high-IRLRPI patients demonstrated pazopanib sensitivity, correlating with established progression-free survival (PFS) benefits in ovarian cancer [64]. Thus, pazopanib is recommended for early treatment in those high-risk subtype patients [65]. Interestingly, the analysis revealed that low-risk patients demonstrated enhanced veliparib sensitivity specifically among PARP inhibitors. Therefore, veliparib is recommended for low-risk patients. These results suggest that our model could predict patients' sensitivity to some chemotherapeutic agents and the triage of patients for better treatment outcomes.

Finally, we used machine learning to screen for the IRLRPI typing-specific biomarkers VSTM2L and KIF26B, reported in previous studies. VSTM2L was associated with tumor immunity in a pan-cancer study and was correlated with poor patient prognosis in ovarian cancer [66, 67]. KIF26B was an immune marker for tumors and could predict patient prognosis in various cancers [68]. This gene was also shown to promote proliferation and migratory activity in an OV cell line [69]. VSTM2L and KIF26B exhibited increased expression in the high-IRLRPI cohort, suggesting biomarker utility and partially accounting for worse prognosis in these patients.

Our findings demonstrate that the IRLRPI score has dual utility in predicting immunotherapy response and informing drug selection. Nevertheless, certain limitations of this study must be considered. First, the scoring model has not been clinically validated, and there is no prospective cohort study to further illustrate its actual value in immunotherapy prediction. Second, the metrics used to observe the effects of various treatments in patients are indirect indicators with no actual clinical medication outcomes as validation. These issues will be addressed and further validated before clinical implementation of this model.

In conclusion, by using immune-related lncRNA, we constructed the IRLRPI and demonstrated, through multiple analyses, that typing could assist in predicting immunotherapy responsiveness and chemotherapy drug sensitivity in patients. This may help guide triage of patients and optimize treatment decisions in advance.

Availability of data and materials

The datasets analyzed during the current study are available in the TCGA GDC (https://portal.gdc.cancer.gov/), GTEx (www.gtexportal.org/), GEO (https://www.ncbi.nlm.nih.gov/geo/, GSE9891) and IMvigor210 (http://research-pub.gene.com/IMvigor210CoreBiologies/).

Funding

This work was supported by grants from the National Natural Science Foundation of China (81972422; 82403164; 82073172; 81572546).

Ethical approval

Not applicable, because the data used in this study derive from the public databases TCGA, GTEx, and GEO, where ethical approval was already obtained by the respective database providers. Users can freely access these datasets for research and publication. As our study is based on open-source data, the Shanghai Tenth People's Hospital, Tongji University School of Medicine and Shanghai Key Laboratory of Maternal Fetal Medicine, Shanghai Institute of Maternal-Fetal Medicine and Gynecologic Oncology, Shanghai First Maternity and Infant Hospital, School of Medicine, School of Life Science and Technology, Tongji University do not require additional ethics review, and there are no ethical issues or other conflicts of interest.

Conflict of interest

The authors declare no conflict of interest.

References

1. Momenimovahed Z, Tiznobaik A, Taheri S, Salehiniya H. Ovarian cancer in the world: epidemiology and risk factors. Int J Womens Health 2019; 11: 287-99.
2. Siegel RL, Miller KD, Fuchs HE, Jemal A. Cancer statistics, 2022. CA Cancer J Clin 2022; 72: 7-33.
3. Ott PA, Bang YJ, Piha-Paul SA, et al. T-cell-inflamed gene-expression profile, programmed death ligand 1 expression, and tumor mutational burden predict efficacy in patients treated with pembrolizumab across 20 cancers: KEYNOTE-028. J Clin Oncol 2019; 37: 318-27.
4. Barber E, Matei D. Immunotherapy in ovarian cancer: we are not there yet. Lancet Oncol 2021; 22: 903-5.
5. Odunsi K. Immunotherapy in ovarian cancer. Ann Oncol 2017; 28: viii1-7.
6. Chen Y, Li ZY, Zhou GQ, Sun Y. An immune-related gene prognostic index for head and neck squamous cell carcinoma. Clin Cancer Res 2021; 27: 330-41.
7. Dai Y, Qiang W, Lin K, Gui Y, Lan X, Wang D. An immune-related gene signature for predicting survival and immunotherapy efficacy in hepatocellular carcinoma. Cancer Immunol Immunother 2021; 70: 967-79.
8. Ji Q, Cai Y, Shrestha SM, Shen D, Zhao W, Shi R. Construction and validation of an immune-related gene prognostic index for esophageal squamous cell carcinoma. Biomed Res Int 2021; 2021: 7430315.
9. Sahu A, Singhal U, Chinnaiyan AM. Long noncoding RNAs in cancer: from function to translation. Trends Cancer 2015; 1: 93-109.

10. Huang X, Xiao R, Pan S, et al. Uncovering the roles of long non-coding RNAs in cancer stem cells. J Hematol Oncol 2017; 10: 62.
11. Slack FJ, Chinnaiyan AM. The role of non-coding RNAs in ocology. Cell 2019; 179: 1033-55.
12. Qi P, Zhou XY, Du X. Circulating long non-coding RNAs in cancer: current status and future perspectives. Mol Cancer 2016; 15: 39.
13. Arun G, Diermeier SD, Spector DL. Therapeutic targeting of long non-coding RNAs in cancer. Trends Mol Med 2018; 24: 257-77.
14. Eptaminitaki GC, Stellas D, Bonavida B, Baritaki S. Long non-coding RNAs (lncRNAs) signaling in cancer chemoresistance: from prediction to druggability. Drug Resist Update 2022; 65: 100866.
15. Zhang L, Xu X, Su X. Noncoding RNAs in cancer immunity: functions, regulatory mechanisms, and clinical application. Mol Cancer 2020; 19: 48.
16. Atianand MK, Caffrey DR, Fitzgerald KA. Immunobiology of long noncoding RNAs. Annu Rev Immunol 2017; 35: 177-98.
17. Zhang Y, Mao Q, Xia Q, et al. Noncoding RNAs link metabolic reprogramming to immune microenvironment in cancers. J Hematol Oncol 2021; 14: 169.
18. Xu J, Shi A, Long Z, et al. Capturing functional long non-coding RNAs through integrating large-scale causal relations from gene perturbation experiments. EBioMedicine 2018; 35: 369-80.
19. Wu J, Li J, Zhu G, et al. Clinical features of maintenance hemodialysis patients with 2019 novel coronavirus-infected pneumonia in Wuhan, China. Clin J Am Soc Nephrol 2020; 15: 1139-45.
20. Liu J, Mei J, Wang Y, et al. Development of a novel immune-related lncRNA signature as a prognostic classifier for endometrial carcinoma. Int J Biol Sci 2021; 17: 448-59.
21. Yu W, Ma Y, Hou W, et al. Identification of immune-related lncRNA prognostic signature and molecular subtypes for glioblastoma. Front Immunol 2021; 12: 706936.
22. Sun X, Li S, Lv X, et al. Immune-related long non-coding RNA constructs a prognostic signature of ovarian cancer. Biol Proced Online 2021; 23: 24.
23. Peng Y, Wang H, Huang Q, Wu J, Zhang M. A prognostic model based on immune-related long noncoding RNAs for patients with epithelial ovarian cancer. J Ovarian Res 2022; 15: 8.
24. Charoentong P, Finotello F, Angelova M, et al. Pan-cancer immunogenomic analyses reveal genotype-immunophenotype relationships and predictors of response to checkpoint blockade. Cell Rep 2017; 18: 248-62.
25. Necchi A, Joseph RW, Loriot Y, et al. Atezolizumab in platinum-treated locally advanced or metastatic urothelial carcinoma: post-progression outcomes from the phase II IMvigor210 study. Ann Oncol 2017; 28: 3044-50.
26. Mariathasan S, Turley SJ, Nickles D, et al. TGFbeta attenuates tumour response to PD-L1 blockade by contributing to exclusion of T cells. Nature 2018; 554: 544-8.
27. Mayakonda A, Lin DC, Assenov Y, Plass C, Koeffler HP. Maftools: efficient and comprehensive analysis of somatic variants in cancer. Genome Res 2018; 28: 1747-56.
28. Geeleher P, Cox N, Huang RS. pRRophetic: an R package for prediction of clinical chemotherapeutic response from tumor gene expression levels. PLoS One 2014; 9: e107468.
29. Wilkerson MD, Hayes DN. ConsensusClusterPlus: a class discovery tool with confidence assessments and item tracking. Bioinformatics 2010; 26: 1572-3.
30. Tibshirani R. The lasso method for variable selection in the Cox model. Stat Med 1997; 16: 385-95.
31. Sanz H, Valim C, Vegas E, Oller JM, Reverter F. SVM-RFE: selection and visualization of the most relevant features through non-linear kernels. BMC Bioinformatics 2018; 19: 432.
32. Tang Z, Li C, Kang B, Gao G, Li C, Zhang Z. GEPIA: a web server for cancer and normal gene expression profiling and interactive analyses. Nucleic Acids Res 2017; 45: W98-102.
33. Lanczky A, Gyorffy B. Web-based survival analysis tool tailored for medical research (KMplot): development and implementation. J Med Internet Res 2021; 23: e27633.
34. Uhlen M, Fagerberg L, Hallstrom BM, et al. Proteomics. Tissue-based map of the human proteome. Science 2015; 347: 1260419.
35. Chan TA, Yarchoan M, Jaffee E, et al. Development of tumor mutation burden as an immunotherapy biomarker: utility for the oncology clinic. Ann Oncol 2019; 30: 44-56.
36. Liu L, Bai X, Wang J, et al. Combination of TMB and CNA stratifies prognostic and predictive responses to immunotherapy across metastatic cancer. Clin Cancer Res 2019; 25: 7413-23.
37. Polastro L, Closset C, Kerger J. Immunotherapy in gynecological cancers: where are we? Curr Opin Oncol 2020; 32: 459-70.
38. Mauricio D, Zeybek B, Tymon-Rosario J, Harold J, Santin AD. Immunotherapy in cervical cancer. Curr Oncol Rep 2021; 23: 61.
39. Li Y, Huo FF, Wen YY, Jiang M. Screening and identification of an immune-associated lncRNA prognostic signature in ovarian carcinoma: evidence from bioinformatic analysis. Biomed Res Int 2021; 2021: 6680036.
40. Pan X, Bi F. A potential immune-related long non-coding RNA prognostic signature for ovarian cancer. Front Genet 2021; 12: 694009.
41. Yang X, Zhou S, Li C, et al. Downregulation of LEMD1-AS1 and its influences on the diagnosis, prognosis, and immune infiltrates of epithelial ovarian cancer. Dis Markers 2022; 2022: 6408879.
42. Jing L, Gong M, Lu X, Jiang Y, Li H, Cheng W. LINC01127 promotes the development of ovarian tumors by regulating the cell cycle. Am J Transl Res 2019; 11: 406-17.
43. Xu Q, Lin YB, Li L, Liu J. LncRNA TLR8-AS1 promotes metastasis and chemoresistance of ovarian cancer through enhancing TLR8 mRNA stability. Biochem Biophys Res Commun 2020; 526: 857-64.
44. Yang J, Wang WG, Zhang KQ. LINC00452 promotes ovarian carcinogenesis through increasing ROCK1 by sponging miR-501-3p and suppressing ubiquitin-mediated degradation. Aging 2020; 12: 21129-46.
45. Wang L, Ye TY, Wu H, Chen SY, Weng JR, Xi XW. LINC00702 accelerates the progression of ovarian cancer through interacting with EZH2 to inhibit the transcription of KLF2. Eur Rev Med Pharmacol Sci 2019; 23: 201-8.
46. Nowak M, Klink M. The role of tumor-associated macrophages in the progression and chemoresistance of ovarian cancer. Cells 2020; 9: 1299.
47. Napoletano C, Ruscito I, Bellati F, et al. Bevacizumab-based chemotherapy triggers immunological effects in responding multi-treated recurrent ovarian cancer patients by favoring the recruitment of effector T cell subsets. J Clin Med 2019; 8: 380.
48. Hornburg M, Desbois M, Lu S, et al. Single-cell dissection of cellular components and interactions shaping

the tumor immune phenotypes in ovarian cancer. Cancer Cell 2021; 39: 928-44 e6.
49. Cai D, Li J, Liu D, et al. Tumor-expressed B7-H3 mediates the inhibition of antitumor T-cell functions in ovarian cancer insensitive to PD-1 blockade therapy, Cell Mol Immunol 2020; 17: 227-36.
50. Leung CS, Yeung TL, Yip KP, et al. Cancer-associated fibroblasts regulate endothelial adhesion protein LPP to promote ovarian cancer chemoresistance. J Clin Invest 2018; 128: 589-606.
51. Zhang M, Chen Z, Wang Y, Zhao H, Du Y. The role of cancer-associated fibroblasts in ovarian cancer. Cancers 2022; 14: 2637.
52. Duong E, Fessenden TB, Lutz E, et al. Type I interferon activates MHC class I-dressed CD11b(+) conventional dendritic cells to promote protective anti-tumor CD8(+) T cell immunity. Immunity 2022; 55: 308-23 e9.
53. Yu R, Zhu B, Chen D. Type I interferon-mediated tumor immunity and its role in immunotherapy. Cell Mol Life Sci 2022; 79: 191.
54. Zitvogel L, Galluzzi L, Kepp O, Smyth MJ, Kroemer G. Type I interferons in anticancer immunity. Nat Rev Immunol 2015; 15: 405-14.
55. Zagorulya M, Yim L, Morgan DM, et al. Tissue-specific abundance of interferon-gamma drives regulatory T cells to restrain DC1-mediated priming of cytotoxic T cells against lung cancer. Immunity 2023; 56: 386-405.
56. Cha JH, Chan LC, Li CW, Hsu JL, Hung MC. Mechanisms controlling PD-L1 expression in cancer. Mol Cell 2019; 76: 359-70.
57. Matulonis UA, Shapira R, Santin A, et al. Final results from the KEYNOTE-100 trial of pembrolizumab in patients with advanced recurrent ovarian cancer. J Clin Oncol 2020; 38: 6005.
58. Moore KN, Bookman M, Sehouli J, et al. Atezolizumab, bevacizumab, and chemotherapy for newly diagnosed stage III or IV ovarian cancer: placebo-controlled randomized phase III trial (IMagyn050/GOG 3015/ENGOT-OV39). J Clin Oncol 2021; 39: 1842-55.
59. Pujade-Lauraine E, Fujiwara K, Ledermann JA, et al. Avelumab alone or in combination with chemotherapy versus chemotherapy alone in platinum-resistant or platinum-refractory ovarian cancer (JAVELIN Ovarian 200): an open-label, three-arm, randomised, phase 3 study. Lancet Oncol 2021; 22: 1034-46.
60. Guo JN, Chen D, Deng SH, et al. Identification and quantification of immune infiltration landscape on therapy and prognosis in left- and right-sided colon cancer. Cancer Immunol Immunother 2022; 71: 1313-30.
61. Song P, Li W, Guo L, Ying J, Gao S, He J. Identification and validation of a novel signature based on NK cell marker genes to predict prognosis and immunotherapy response in lung adenocarcinoma by integrated analysis of single-cell and bulk RNA-sequencing. Front Immunol 2022; 13: 850745.
62. Zheng M, Hu Y, Gou R, et al. Development of a seven-gene tumor immune microenvironment prognostic signature for high-risk grade III endometrial cancer. Mol Ther Oncolytics 2021; 22: 294-306.
63. Jardim DL, Goodman A, de Melo Gagliato D, Kurzrock R. The challenges of tumor mutational burden as an immunotherapy biomarker. Cancer Cell 2021; 39: 154-73.
64. du Bois A, Floquet A, Kim JW, et al. Incorporation of pazopanib in maintenance therapy of ovarian cancer. J Clin Oncol 2014; 32: 3374-82.
65. Mirza MR, Coleman RL, Gonzalez-Martin A, et al. The forefront of ovarian cancer therapy: update on PARP inhibitors. Ann Oncol 2020; 31: 1148-59.
66. Zhang S, Xiong H, Yang J, Yuan X. Pan-cancer analysis reveals the multidimensional expression and prognostic and immunologic roles of VSTM2L in cancer. Front Mol Biosci 2021; 8: 792154.
67. Yuan H, Yu Q, Pang J, Chen Y, Sheng M, Tang W. The value of the stemness index in ovarian cancer prognosis. Genes (Basel) 2022; 13: 993.
68. Sun F, Lian Y, Wang J, Hu L, Luo J, Yu J. KIF26B in the prognosis and immune biomarking of various cancers: a pan-cancer study. J Oncol 2022; 2022: 4829697.
69. Yang X, Zhang L, Xie L. Upregulation of KIF26B, cell migration and proliferation of human ovarian cancer cell lines in vitro, and patient outcomes from human bioinformatic analysis. Med Sci Monit 2018; 24: 3863-72.